




Article

# Metal-Selective Processing from the Los Sulfatos Porphyry-Type Deposit in Chile: Co, Au, and Re Recovery Workflows Based on Advanced Geochemical Characterization

Germán Velásquez <sup>1,\*</sup> , Humberto Estay <sup>1</sup> , Iván Vela <sup>2</sup>, Stefano Salvi <sup>3</sup>  and Marcial Pablo <sup>2</sup>

<sup>1</sup> Advanced Mining Technology Center (AMTC), FCFM, Universidad de Chile, Santiago 8370451, Chile; humberto.estay@amtc.cl

<sup>2</sup> Superintendence of Geology, Los Bronces Underground Project, Anglo American Sur S.A., Santiago 7550103, Chile; ivan.vela@angloamerican.com (I.V.); marcial.pablof@angloamerican.com (M.P.)

<sup>3</sup> Géosciences Environnement Toulouse (GET), Université de Toulouse, CNRS, GET, IRD, OMP, 14 Av. Edouard Belin, 31400 Toulouse, France; stefano.salvi@get.omp.eu

\* Correspondence: gevelasqueza@gmail.com

Received: 20 May 2020; Accepted: 9 June 2020; Published: 11 June 2020



**Abstract:** Sulfides extracted from porphyry-type deposits can contain a number of metals critical for the global energy transition, e.g., Co and precious metals such as Au and Re. These metals are currently determined on composite mineral samples, which commonly results in their dilution. Thus, it is possible that some metals of interest are overlooked during metallurgical processing and are subsequently lost to tailings. Here, an advanced geochemical characterization is implemented directly on metal-bearing sulfides, determining the grade of each targeted trace metal and recognizing its specific host mineral. Results show that pyrite is a prime host mineral for Co (up to 24,000 ppm) and commonly contains Au (up to 5 ppm), while molybdenite contains high grades of Re (up to 514 ppm) and Au (up to 31 ppm). Both minerals represent around 0.2% of the mineralized samples. The dataset is used to evaluate the possibility of extracting trace metals as by-products during Cu-sulfide processing, by the addition of unit operations to conventional plant designs. A remarkable advantage of the proposed workflows is that costs of mining, crushing, and grinding stages are accounted for in the copper production investments. The proposed geochemical characterization can be applied to other porphyry-type operations to improve the metallic benefits from a single deposit.

**Keywords:** cobalt supply; rhenium; gold; by-products; pyrite processing; geo-metallurgy; porphyry-type mining; green mining

## 1. Introduction

Nowadays, metal resources are more crucial than ever to current global energy transition efforts [1–4], especially metals needed for the development of clean energy technologies [5,6]. Demand for these metals will increase in the coming years, with copper (Cu) being in greatest demand worldwide, estimated up to 40 times greater by 2100 [7]. This will be accompanied by other metals such as cobalt (Co), silver (Ag), tellurium (Te), rare earth elements (REEs), all of which are considered critical because of the risk they pose to supply [5,8]. Constraints on Cu supply focus on the expected decline in ore grades [9], which implies that significantly more mine material will have to be mined and processed to produce the same amount of metal. Thus, a significant challenge to the copper industry would be to move from traditional Cu ( $\pm$  Mo  $\pm$  Au) mining to a highly efficient multi-metallic operation [10]. This would allow the exploitation of all of the metal resources contained in a single mineral deposit, while at the same time minimizing the amount of waste generated [11].

Critical and precious metals such as Co, Au, and Re, not to mention Ag, are systematically reported as by-products in porphyry-Cu-Mo deposits worldwide, with metal grades averaging at around 0.5 g/t [10,12–14]. However, an issue that must be addressed in mineral characterization protocols is that the minerals that host each specific metal of interest are not recognized, which is a crucial piece of information for metallurgical ore processing [15,16]. This issue can be explained by the following considerations: (i) mineral characterization is focused on copper ore, i.e., Cu oxides and sulfides, and does not include all metal-bearing minerals [10]; (ii) geochemical analyses are carried out by taking a sample of the whole mineralized rock, i.e., a sample containing ores and barren minerals, resulting in the dilution of some trace metals to concentrations that are below detection limits [10]; and (iii) mineral paragenesis is predicted from whole-rock geochemical data [17], instead of being determined by conventional and more-sophisticated microscopic methods.

To evaluate the economic metal content of a porphyry-type deposit, Velásquez et al. [10] proposed a high-resolution mineral and geochemical characterization, which should allow efficient determination of the grade of targeted metals and recognition of specific host minerals. The data obtained include both the metal concentration (grade) and the mode of occurrence for each metal (e.g., visible, invisible, in the structure, etc.) [10], which is valuable information for selective metal treatment.

In this paper, we present the results of a high-resolution geochemical characterization performed *in situ* on sulfides (i.e., bornite, chalcopyrite, molybdenite, and pyrite) from Cu-mineralized samples belonging to a porphyry-type deposit. Geochemical characterization is intended to determine and quantify the Co, Au, and Re, as well as Ag, Te, and As content of sulfides, rather than measuring trace elements in the whole rock. The resulting dataset is used to: (1) determine the preferred host sulfide for each selected trace metal; (2) highlight the difference between advanced and operational geochemical characterization; and (3) discuss how high-resolution characterization can support more appropriate Cu ore processing plant design, focused on the supply of critical and precious metals, in addition to the major compounds, i.e., Cu and Mo. The proposed metallurgical workflows can be implemented in mining operations to move from traditional Cu ( $\pm$  Mo) mining to high-performance multi-metallic activity in porphyry-type mines.

As a case study, we have chosen the Los Sulfatos deposit [18,19], located in the Chilean Central Andes. Managed by Anglo American Sur, S.A., Los Sulfatos is a world-class deposit (>45 Mt of contained copper) [10]. It is part of the Los Bronces–Rio Blanco–Los Sulfatos porphyry Cu-Mo system [18–20] (Figure 1), which is considered having the highest copper endowment in the Earth's crust (>200 Mt of contained copper) [18–20]. The main ore minerals found in the deposit are Cu  $\pm$  Mo- sulfides, predominantly chalcopyrite, bornite, and some molybdenite [18,19]. At present, the deposit is in its preliminary development stages as the Los Bronces underground mining project. The deposit contains more than 3.9 billion tons of mine-material enriched in Cu-Mo-sulfides and grading 1.14% Cu [10], which will be extracted throughout the duration of the mine's life. The final marketing product expected to be generated during the metallurgical processing is a sulfide (bulk and selective) flotation concentrate, while the rest of the extracted mine-material will be removed to tailings [10]. The fact that Anglo American Sur S.A. is evaluating the conditions for mining operation development in the coming years for the Los Sulfatos deposit, offers a rare opportunity to propose a multi-metal metallurgical processing in a porphyry Cu-Mo mining operation by implementing the high-resolution characterization proposed by Velásquez et al. [10]. The case study is focused on porphyry-types deposits due to the increased need for copper in the coming years, which implies that the mineralized material will be extracted and processed to supply this metal and, therefore, the goal for mining geologists is to improve the metallic benefits drawn from each deposit.

In this study, we will focus on determining Co, Re, and Au occurrences in the sulfides. The specific choice of these commodities arises from the following considerations: (i) Cobalt is a key metal in the production of rechargeable lithium (Li)-ion batteries [21,22]; given that Chile is one of the world's leading suppliers of Li [23,24], the possibility of producing both Co and Li would be highly strategic for the country, as it would become a leader in the high-tech clean energy industry. (ii) Rhenium is

contained in molybdenite (up to 4.7 wt.% Re), a common sulfide in porphyry-type deposits [8,13,25]. However, Re concentrations could not be assessed during operational geochemical characterization, because this procedure is performed on composite samples by whole-rock analysis. This implies that Re would not be included in the mining planning being recovered later from refineries. (iii) Gold is currently determined by bulk assays [12], but practically no mineral characterization is performed on its host mineral. As a result, the metallic Au contents would not be exploited in the metallurgical treatment and would instead be lost to tailings [10]. This is especially relevant in the case of invisible occurrences of Au [26], in which Au can occur as nanoparticles of sulfosalts or in the structure lattice.

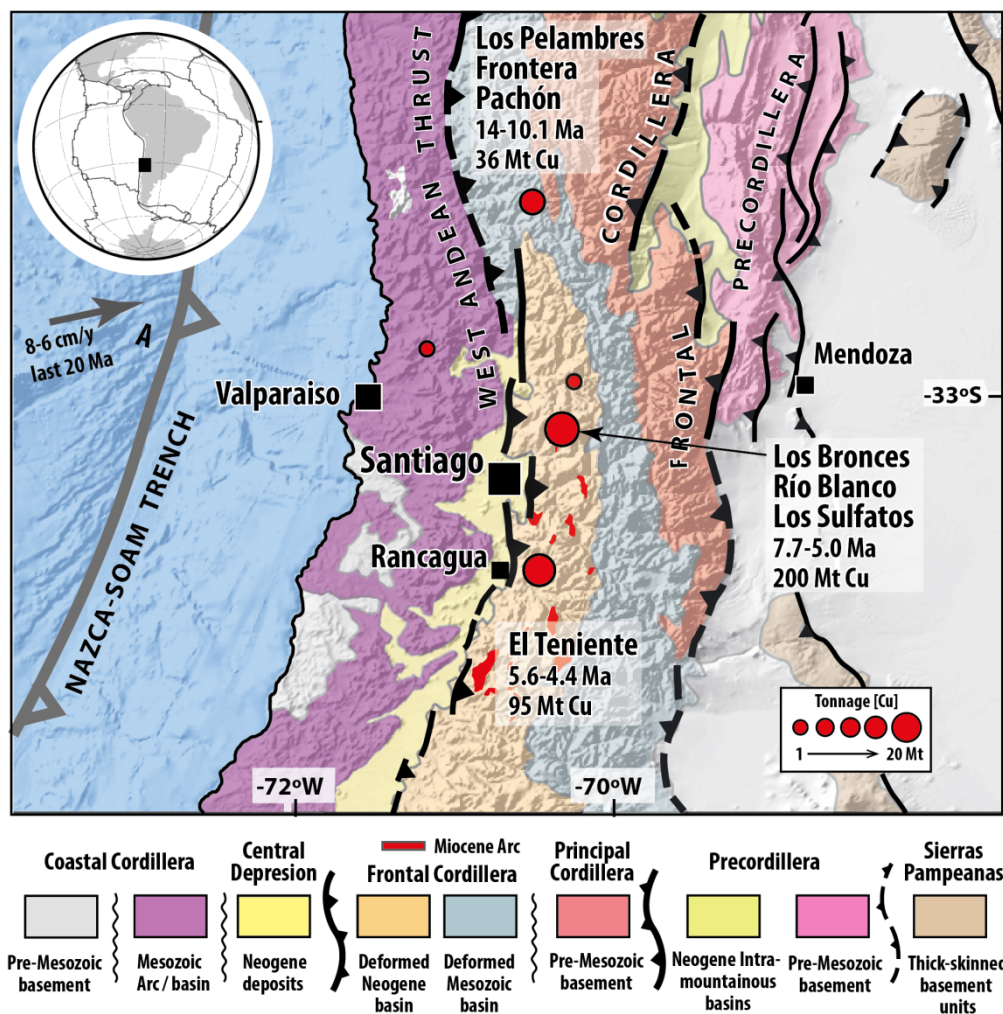


**Figure 1.** Physiography and first-order tectonic setting of the Central Andes showing the geological framework of the Río Blanco–Los Bronces–Los Sulfatos Cu–Mo porphyry system (modified from reference [27]).

## 2. Samples and Analytical Protocol

For this study, we sampled ten drill cores of mineralized material from the Los Sulfatos deposit at depths from 100 to 800 m, which are located in the expected exploitation area to be developed as the Los Bronces underground project. From these drill cores, fifteen 5 m-mineralized intervals were selected and two hand-picked samples were collected from each interval (Figure 2). It is important to note that each 5 m interval corresponds to a composite-sample analyzed by whole-rock chemical analysis, which is a routinely analytical procedure in the mining industry (Figure 2a). The goal of that correspondence is to compare the whole-rock geochemical data with the obtained results from an advanced micro-chemical characterization (Figure 2b). Thus, thirty representative samples

were collected from four mineralized zones, *Min-Zones*, defined at the Los Sulfatos deposit [10], i.e., high-chalcopyrite (CPY-H), low-chalcopyrite (CPY-L), high-bornite (BRN-H), and low-bornite (BRN-L). All of these are developed in hydrothermal and magmatic breccias. Of these samples, fifteen were found to be suitable for high-resolution investigation of mineral and geochemical characterization. About one hundred sulfide crystals, including chalcopyrite, bornite, molybdenite, and pyrite (Figure 2b), were analyzed to determine their trace-metal content, focusing on critical, precious, and deleterious metals, i.e., Co, Au, Re, plus Ag, Te, and As. Mineralogical and micro-chemical studies were carried out at the Géosciences Environnement Toulouse (GET) laboratory in Toulouse, France by the application of conventional practices used for mineral protocols. These practices include petrographic and scanning electron microscope (SEM) descriptions, which were combined with more sophisticated techniques applied for micro-chemical mineral characterization [10], such as the laser ablation-inductively coupled plasma-mass spectrometry [28]. The analytical protocol is summarized below.

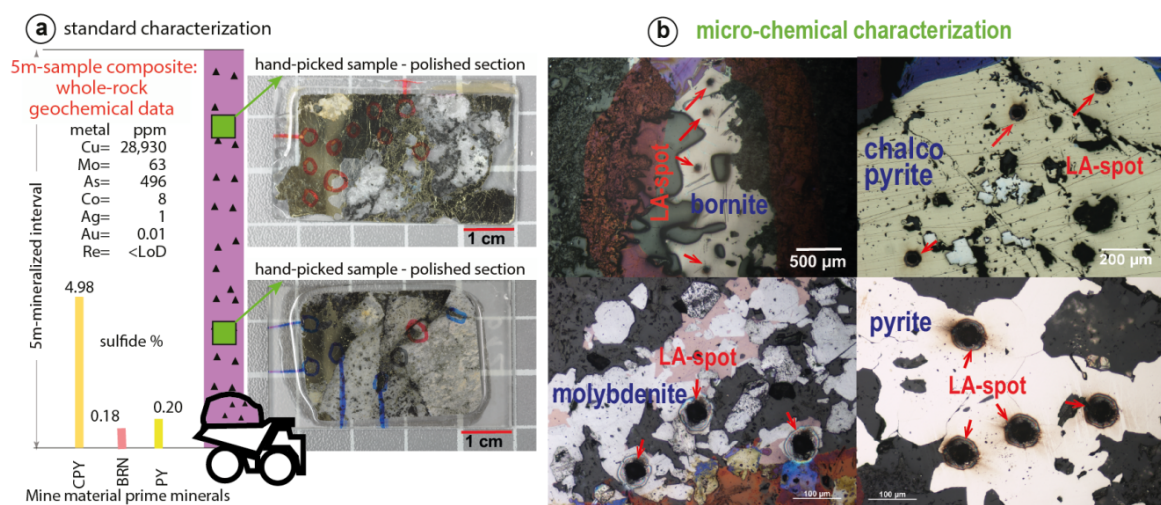


**Figure 2.** (a) Schematic diagram illustrating a selected 5 m-mineralized interval, highlighting (green filled squares) the locations of collected samples. Metal concentrations obtained from bulk analyses are indicated on the left side. Photographs of the 200 μm-thick polished sections corresponding to the hand-picked samples are shown on the right. (b) Photomicrographs under reflected light showing the different sulfides types analyzed by LA-ICP-MS, highlighting the locations of laser-ablation spots (LA-spot). Photomicrographs were taken after laser ablation analysis.

- Logging of a 5 m-mineralized interval of each selected drill-core, from which a core-sample was collected and prepared to design a 200 μm-thick polished section (Figure 2a);
- Identification of sulfide minerals by petrographic studies [10,29] (Figure 2a), using a polarizing microscope Nikon Eclipse LV100POL (Nikon instruments Europe, Amsterdam, The Netherlands) in reflected and transmitted light, equipped with 2×, 5×, 10×, 20× and 50× objectives;
- Characterization of metal-bearing mineral inclusions in sulfides [10,29], using a JEOL6360LV scanning electron microscopy (JEOL Ltd., Tokyo, Japan) coupled to an energy-dispersive X-ray spectrometer (SDD Bruker 129 eV) (Bruker Corporation, Billerica, MA, USA), itself equipped to acquire images in backscattered electron (BSE) mode at an acceleration voltage of 20 kV;
- Determination of trace metal concentrations in sulfides by in situ micro-chemical analyses, including electron micro-probe (EPM) and laser ablation (LA-ICP-MS) analyses [10,29], using a CAMECA SX5 microprobe (CAMECA SX5, Cameca, Gennevilliers, France), combined with a Ti: sapphire femtosecond (fs) laser couple to a quadrupole ICP-MS. To provide a sense of reproducibility of the LA-ICP-MS analysis, several spots were ablated on each single sulfide crystal, avoiding the consideration of outstanding concentration values (Figure 2b). Detection limits for trace element quantifications were calculated as three times the background standard deviation

value. At GET, the tuning routine is optimized to reduce production of molecular oxide species (typically  $^{232}\text{Th}^{16}\text{O}^{232}\text{Th} < 1\%$ ) and doubly charged ion species (typically  $^{140}\text{Ce}^{++}/^{140}\text{Ce}^{+} < 2\%$ ). This allows an analytical precision of  $< 15\%$  for the relative standard deviation (RSD) to be reached [30,31]. The gas blank is measured for 30 s before switching on the laser for 60 s. Raw data were processed online using the GLITTER software package (4.0, ARC National Key Centre for Geochemical Evolution and Metallogeny of Continents, Macquarie University, Sydney, Australia) (e.g., [32]), using certified reference materials, such as pyrrhotite-Po-726 [33], an in-house natural chalcopyrite, Cpy-RM [30], and NIST SRM 610 [34], as external calibrators, in bracketing mode standard-sample-standard. The following isotopes were monitored:  $^{33}\text{S}$ ,  $^{34}\text{S}$ ,  $^{56}\text{Fe}$ ,  $^{57}\text{Fe}$ ,  $^{59}\text{Co}$ ,  $^{63}\text{Cu}$ ,  $^{75}\text{As}$ ,  $^{95}\text{Mo}$ ,  $^{107}\text{Ag}$ ,  $^{125}\text{Te}$ ,  $^{182}\text{W}$ ,  $^{185}\text{Re}$ ,  $^{197}\text{Au}$ . These isotopes were selected to avoid possible argide interferences ( $\text{MeAr}^+$ ), where Me corresponds to a base metal such as  $^{59}\text{Co}$  and  $^{63}\text{Cu}$ , in our study case. Analytical routines and conditions are described in detail in references [10,29–31].

### 3. High-Resolution Geochemical Characterization of Sulfides

In this study, we focus on determining the presence of critical and precious metals in sulfides, i.e., chalcopyrite, bornite, molybdenite, and pyrite from a porphyry-type deposit, taking Cu-mineralized material from drill-holes as study samples. Around one-hundred sulfide crystals were selected from the four *Min-Zones* defined at the Los Sulfatos deposit [10] and were subjected to in-depth investigations. Detailed petrographic and textural observations performed on sulfide crystals evidence two different sulfide metallogenic units in the mineralized blocks: (1) an association consisting of bornite–chalcopyrite  $\pm$  molybdenite (BRN–CPY  $\pm$  MOL; Figure 3a); and (2) an association formed by chalcopyrite  $\pm$  pyrite (CPY  $\pm$  PY; Figure 3b). The two metallogenic units are spatially related with the *Min-Zones*, recognized in the geological 3D model for the Los Sulfatos deposit.

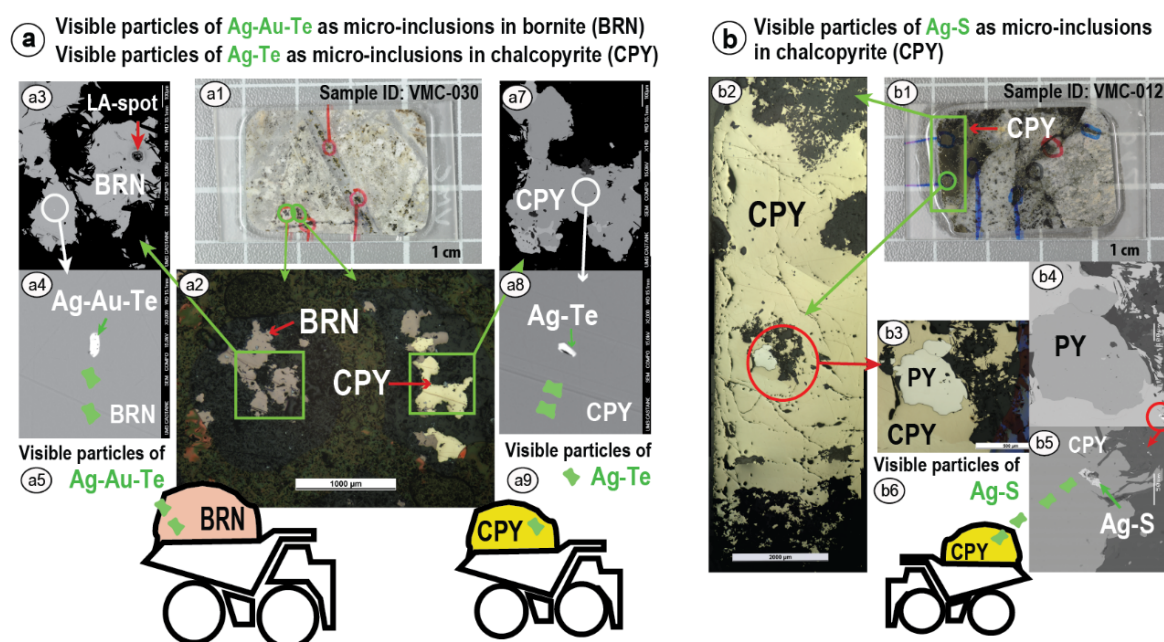


**Figure 3.** (a) Microphotograph under reflected light (a2) and BSE images (a3,a4,a7,a8) deciphering the occurrence of visible particles of Ag-Au-Te and Ag-Te, found as micron-sized inclusions in bornite and chalcopyrite, respectively. The expected final destination of these particles is also shown (a5,a9). (b) Microphotographs under reflected light (b2,b3) and BSE images (b4,b5) showing the occurrence of Ag-S visible particles, found as micron-sized inclusions in chalcopyrite. The estimated final destination for these metallic particles is also the flotation concentrates (b6). CPY: chalcopyrite, BRN: bornite, and PY: pyrite.

### 3.1. Visible Metal Content in the Sulfide Units

Visible metals correspond to the micron-sized (up to 1  $\mu\text{m}$ ) particles that can be determined by optical microscope or SEM. They occur as metal-bearing inclusions in the sulfides [10,29]. In the BRN–CPY  $\pm$  MOL unit, recognized metallic particles include sulfosalts of Ag–Te (e.g., hessite:  $\text{Ag}_2\text{Te}$ ) and Ag–Au–Te (e.g., sylvanite:  $(\text{Ag}, \text{Au})\text{Te}_2$ ). Ag–Te particles occur as inclusions in chalcopyrite, while Ag–Au–Te particles are preferentially included in bornite (Figure 3a). Studied molybdenite crystals were found to be free of visible metallic inclusions.

In the CPY  $\pm$  PY unit, sulfosalts of Ag–S (e.g., acanthite:  $\text{Ag}_2\text{S}$ ) were found as micron-sized inclusions in chalcopyrite (Figure 3b), whereas pyrite, which crystallizes intergrown with chalcopyrite, is almost free of visible metallic inclusions.

The association between the sulfosalt and their corresponding hosting sulfide implies that these metallic micron-sized particles (Figure 3) will accumulate in the sulfide flotation concentrates during the metallurgical processing circuits.

### 3.2. Invisible Trace-Metal Content in the Sulfide Units

This corresponds to the metal content which cannot be determined by SEM and EPM analyses, because the concentration is below the detection limits of these techniques. To evaluate the presence of selected trace metals, i.e., Co, Au, Re, plus Ag, Te, W, and As in the ore sulfides, 161 LA-ICP-MS analyses were performed. Of these, 54 analytical spots were ablated on sulfides from the CPY  $\pm$  PY unit, and 107 spots on sulfides from the BRN–CPY  $\pm$  MOL unit. The analytical routine included determination of As, because it is a deleterious metal during copper ore processing [35], and its occurrence can influence the price of sulfide flotation concentrates. Chalcopyrite, bornite, and pyrite were analyzed to determine Co, Au, Ag, Te, and As, while molybdenite was analyzed for Re, and Au, (plus W), because they represent the prime trace metals that could be concentrated in molybdenite crystals [36]. Invisible metal content can occur as mineral micro- and nano-particles or be included in the lattice structure [37].

#### 3.2.1. Bornite–Chalcopyrite $\pm$ Molybdenite Unit

The results of LA-ICP-MS analyses (Table 1) show that Ag is preferentially contained in bornite, with an average value of 103.3 ppm (up to 316 ppm Ag) and that it is correlated with the highest concentrations of Te (up to 129 ppm), and Au (up to 1 ppm). In chalcopyrite crystals, Ag and Te contents reach up to 22 and 14 ppm, respectively, while Au concentrations are below the detection limit of the LA-ICP-MS (DL = 0.05 ppm). Chemical results are in agreement with the mineralogical results, i.e., visible micron-sized particles of Ag–Au–Te are commonly contained in bornite, and visible particles of Ag–Te are mostly found in chalcopyrite. The average concentration of selected trace metals in molybdenite ( $n = 5$  spots) is: Re = 349 ppm (up to 514 ppm), Au = 7 ppm (up to 31 ppm), and W = 12.6 ppm (up to 31 ppm).

Time-resolved LA-ICP-MS profiles were evaluated to determine the mode of occurrence of trace Ag, Te, and Au in bornite and chalcopyrite, and to compare them with mineralogical observations. In the bornite analyses, the spectra for Ag, Au, and Te mimic each other (Figure 4a), and their signals show a spike above background. This indicates that these elements are likely to occur as micro- and nano-particles of Au–Ag–Te [10,29,37,38], in addition to the visible micron-sized particles observed as mineral inclusions. In the chalcopyrite analyses, Ag and Te show correlated signals (Figure 4b), while the Au spectra is in the background, implying the occurrence of Ag–Te micro- and nano-particles [10,29,37,38]. However, some LA-ICP-MS spectra for bornite (Figure 4c), as well as chalcopyrite, display Ag signals higher than those displayed for the other metals (e.g., Te and Au) by at least two orders of magnitude, showing that at least a part of the invisible Ag is contained also in the lattice of sulfides.

**Table 1.** Concentrations for Co, As, Ag, Te, and Au (in ppm) determined by in situ LA-ICP-MS analysis on selected bornite and chalcopyrite crystals.

Sample	Sulfide	Spot	Co (ppm) <i>DL = 0.1</i>	As (ppm) <i>DL = 0.1</i>	Ag (ppm) <i>DL = 0.05</i>	Te (ppm) <i>DL = 0.1</i>	Au (ppm) <i>DL = 0.02</i>
CMP-005	BRN	<i>n</i> = 19	<b>1.3 ± 1.4</b> (< <i>DL</i> -6.2)	<b>1.2 ± 1.0</b> (1.0-4.5)	<b>61.5 ± 7.6</b> (60.2-80.1)	<b>8.9 ± 4.8</b> (12.2-16.6)	<b>0.5 ± 0.3</b> (< <i>DL</i> -1.0)
CMP-006	BRN	<i>n</i> = 8	<b>0.3 ± 0.2</b> (< <i>DL</i> -0.6)	<b>1.1 ± 0.2</b> (1.0-1.3)	<b>50.8 ± 15.9</b> (64.0-76.3)	<b>5.5 ± 3.5</b> (5.2-11.1)	<b>0.6 ± 0.2</b> (< <i>DL</i> -0.6)
CMP-007	BRN	<i>n</i> = 12	<b>0.2 ± 0.1</b> (< <i>DL</i> -0.4)	<b>1.3 ± 0.5</b> (0.8-2.5)	<b>104.5 ± 14.1</b> (72.5-124.4)	<b>7.1 ± 6.1</b> (9.0-24.6)	<b>0.3 ± 0.1</b> (< <i>DL</i> -0.3)
CMP-007	BRN	<i>n</i> = 8	<b>1.1 ± 0.6</b> (< <i>DL</i> -1.3)	<b>6.1 ± 1.9</b> (4.9-9.1)	<b>113.8 ± 34.9</b> (142.8-152.6)	<b>68.9 ± 34.7</b> (29.0-129.0)	< <i>DL</i>
CMP-027	BRN	<i>n</i> = 9	<b>3.7 ± 2.1</b> (< <i>DL</i> -6.2)	<b>7.0 ± 4.5</b> (< <i>DL</i> -11.7)	<b>116.9 ± 60.6</b> (74.1-221.1)	<b>68.9 ± 39.8</b> (10.0-111.0)	< <i>DL</i>
CMP-030	BRN	<i>n</i> = 5	<b>0.6 ± 0.3</b> (< <i>DL</i> -0.9)	<b>1.3 ± 0.4</b> (0.6-1.6)	<b>307.1 ± 12.0</b> (292.4-316.1)	<b>34.7 ± 12.8</b> (19.3-54.9)	<b>0.4 ± 0.2</b> (< <i>DL</i> -0.5)
Bornite		<b><i>n</i> = 61</b>	<b>0.9</b>	<b>2.4</b>	<b>103.3</b>	<b>18.4</b>	<b>0.4</b>
CMP-001	CPY	<i>n</i> = 11	<b>2.4 ± 0.9</b> (0.8-4.0)	<b>1.0 ± 0.9</b> (0.5-3.4)	<b>7.3 ± 5.7</b> (2.9-21.0)	<b>3.3 ± 3.0</b> (1.8-13.7)	< <i>DL</i>
CMP-002	CPY	<i>n</i> = 4	<b>5.4 ± 4.6</b> (0.2-11.4)	<b>10.3 ± 9.3</b> (1.1-23.3)	<b>0.9 ± 0.7</b> (0.1-1.8)	<b>2.2 ± 1.5</b> (0.2-3.8)	< <i>DL</i>
CMP-003	CPY	<i>n</i> = 4	<b>1.0 ± 0.4</b> (0.6-1.5)	<b>11.3 ± 10.0</b> (2.5-21.7)	<b>1.7 ± 0.3</b> (1.4-2.2)	<b>1.2 ± 0.4</b> (0.7-1.5)	< <i>DL</i>
CMP-007	CPY	<i>n</i> = 7	<b>7.9 ± 5.5</b> (1.8-16.9)	<b>2.4 ± 1.2</b> (1.4-4.4)	<b>4.5 ± 4.1</b> (0.2-11.7)	<b>1.6 ± 1.2</b> (0.3-2.5)	< <i>DL</i>
CMP-024	CPY	<i>n</i> = 5	<b>2.6 ± 1.4</b> (2.0-4.0)	<b>4.3 ± 1.5</b> (1.8-5.3)	<b>1.9 ± 1.6</b> (0.6-4.7)	<b>2.9 ± 2.7</b> (0.8-7.4)	< <i>DL</i>
CMP-027	CPY	<i>n</i> = 5	<b>13.4 ± 6.7</b> (8.9-15.9)	<b>5.7 ± 3.3</b> (4.1-6.8)	<b>1.2 ± 0.9</b> (0.6-2.5)	<b>2.0 ± 1.3</b> (1.0-3.0)	< <i>DL</i>
CMP-030	CPY	<i>n</i> = 5	<b>7.5 ± 6.1</b> (2.7-18.1)	<b>1.1 ± 0.8</b> (0.5-2.1)	<b>1.7 ± 1.1</b> (0.3-2.9)	<b>0.8 ± 0.7</b> (0.1-1.6)	< <i>DL</i>
Chalcopyrite		<b><i>n</i> = 41</b>	<b>5.1</b>	<b>3.9</b>	<b>3.2</b>	<b>2.2</b>	< <i>DL</i>

Average values (in bold) ± standard deviation and value range (in brackets) for selected trace-element concentrations. *n*: number of spot analyses. BRN = bornite; CPY = chalcopyrite. *DL*: limit of detection. CMP: critical metal project.

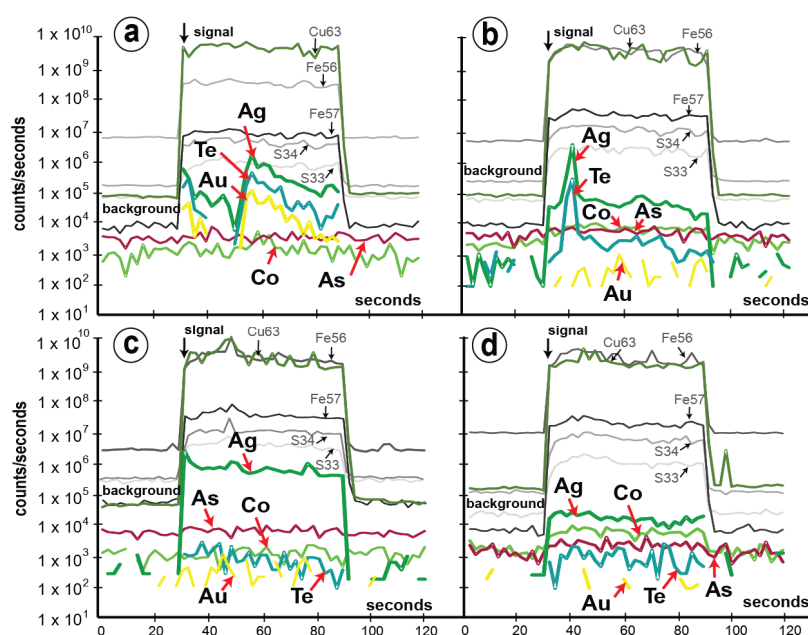


**Figure 4.** LA-ICP-MS patterns (in counts per second) for selected trace-element signals depicting a typical pattern for (a) invisible particles of Ag-Au-Te in bornite; (b) invisible particles of Ag-Te in chalcopyrite; (c,d) invisible silver in the mineral’s lattice of bornite and chalcopyrite, respectively.

### 3.2.2. Chalcopyrite ± Pyrite Unit

Micro-chemical data (Table 2) show that the highest Ag values (up to 42.6 ppm) are contained in chalcopyrite. This is depleted in Te (up to 8.9 ppm) as well as Au (up to 0.07 ppm), in comparison with Cu-sulfides from the unit described previously. LA-ICP-MS profiles for the chalcopyrite analyses (Figure 4d) show a flat pattern for Ag signal well above that of Te, while the Au signal is in the background, which suggests that trace Ag is mostly contained in the mineral's lattice. Pyrite is the strategic Co-host mineral, with an average grade value of 2236 ppm and ranging of up to 24,000 ppm (Table 2). Interestingly, pyrite is also enriched in metallic Au (up to 5 ppm); however, the latter is accompanied by As with an average value of 2801 ppm (up to 6090 ppm) (Table 2). In the last case, Au and As metal content can be hosted in this sulfide's lattice [10].

**Table 2.** Concentrations for Co, As, Ag, Te, and Au (in ppm) determined by in situ LA-ICP-MS analysis on selected chalcopyrite and pyrite crystals.

Sample	Sulfide	Spot	Co (ppm) <i>DL = 0.1</i>	As (ppm) <i>DL = 0.1</i>	Ag (ppm) <i>DL = 0.05</i>	Te (ppm) <i>DL = 0.1</i>	Au (ppm) <i>DL = 0.02</i>
CMP-004	CPY	<i>n</i> = 11	<b>6.4 ± 3.7</b> (< <i>DL</i> -10.1)	<b>14.8 ± 8.3</b> (3.6-24.5)	<b>1.0 ± 0.4</b> (0.4-1.4)	<b>1.1 ± 0.9</b> (0.2-2.9)	<b>0.07 ± 0.02</b> (< <i>DL</i> -0.07)
CMP-009	CPY	<i>n</i> = 5	<b>12.3 ± 12.0</b> (0.2-32.2)	<b>3.3 ± 3.0</b> (1.6-8.6)	<b>12.3 ± 17.0</b> (2.3-42.6)	<b>3.3 ± 2.4</b> (1.3-7.5)	< <i>DL</i>
CMP-011	CPY	<i>n</i> = 7	<b>16.0 ± 3.9</b> (10.9-22.4)	<b>6.0 ± 11.0</b> (1.4-31.7)	<b>2.2 ± 0.3</b> (1.9-2.8)	<b>0.1 ± 0.2</b> (< <i>DL</i> -0.2)	<b>0.07 ± 0.02</b> (< <i>DL</i> -0.07)
CMP-012	CPY	<i>n</i> = 10	<b>0.5 ± 0.3</b> (< <i>DL</i> -0.8)	<b>5.2 ± 3.1</b> (< <i>DL</i> -8.3)	<b>20.8 ± 4.2</b> (15.3-27.0)	<b>4.2 ± 2.2</b> (1.0-8.9)	< <i>DL</i>
CMP-013	CPY	<i>n</i> = 5	<b>14.1 ± 8.0</b> (3.9-26.1)	<b>0.3 ± 0.1</b> (0.2-0.5)	<b>2.5 ± 1.9</b> (1.2-5.8)	<b>0.5 ± 0.3</b> (< <i>DL</i> -0.7)	< <i>DL</i>
Chalcopyrite		<i>n</i> = 38	<b>8.7</b>	<b>7.3</b>	<b>8.3</b>	<b>2.0</b>	<b>0.07</b>
CMP-012	PY	<i>n</i> = 6	<b>7700 ± 6100</b> (172-24,050)	<b>125.4 ± 95.6</b> (1.7-14.9)	< <i>DL</i>	<b>1.4 ± 0.6</b> (< <i>DL</i> -1.8)	< <i>DL</i>
CMP-015	PY	<i>n</i> = 12	<b>354 ± 240</b> (142-747)	<b>3702 ± 2794</b> (0.7-6090)	<b>2.2 ± 1.3</b> (< <i>DL</i> -4.0)	<b>0.8 ± 0.4</b> (< <i>DL</i> -1.6)	<b>0.6 ± 0.4</b> (<0.2-5.0)
Pyrite		<i>n</i> = 16	<b>2236</b>	<b>2801</b>	<b>2.0</b>	<b>0.8</b>	<b>0.6</b>

Average values (in bold) ± standard deviation and value range (in brackets) for selected trace-element concentrations. *n*: number of spot analyses. CPY = chalcopyrite; PY = pyrite. *DL*: limit of detection. CMP: critical metal project.

## 4. Innovation on Metal-Selective Metallurgical Processing

Based on advanced geochemical characterizations of sulfides, two geo-metallurgical units (GMU; Figures 5 and 6) are proposed. These units are focused on Cu + by-products processing: (1) a chalcopyrite–bornite ± molybdenite unit (GMU1; Figure 5), and (2) a chalcopyrite ± pyrite unit (GMU2; Figure 6); both of which correlate with the *Min-Zones* defined at the deposit. However, in the current standard characterization (Figures 5a and 6a) of copper *Min-Zones*, some trace elements are not determined as well as the specific sulfide that hosts each studied metal. From a high-resolution characterization [10] (Figures 5b and 6b), it is possible to determine the trace-metal content of a mineral, including its concentration (metal grade), the host phase, and form of occurrence (e.g., micron-sized particle, nano-particle, or in the lattice). These characteristics are depicted below for sulfides found in each GMU (Figures 5 and 6), focusing on the selected trace metals, i.e., Co, Au, and Re, plus Ag, Te, and As.



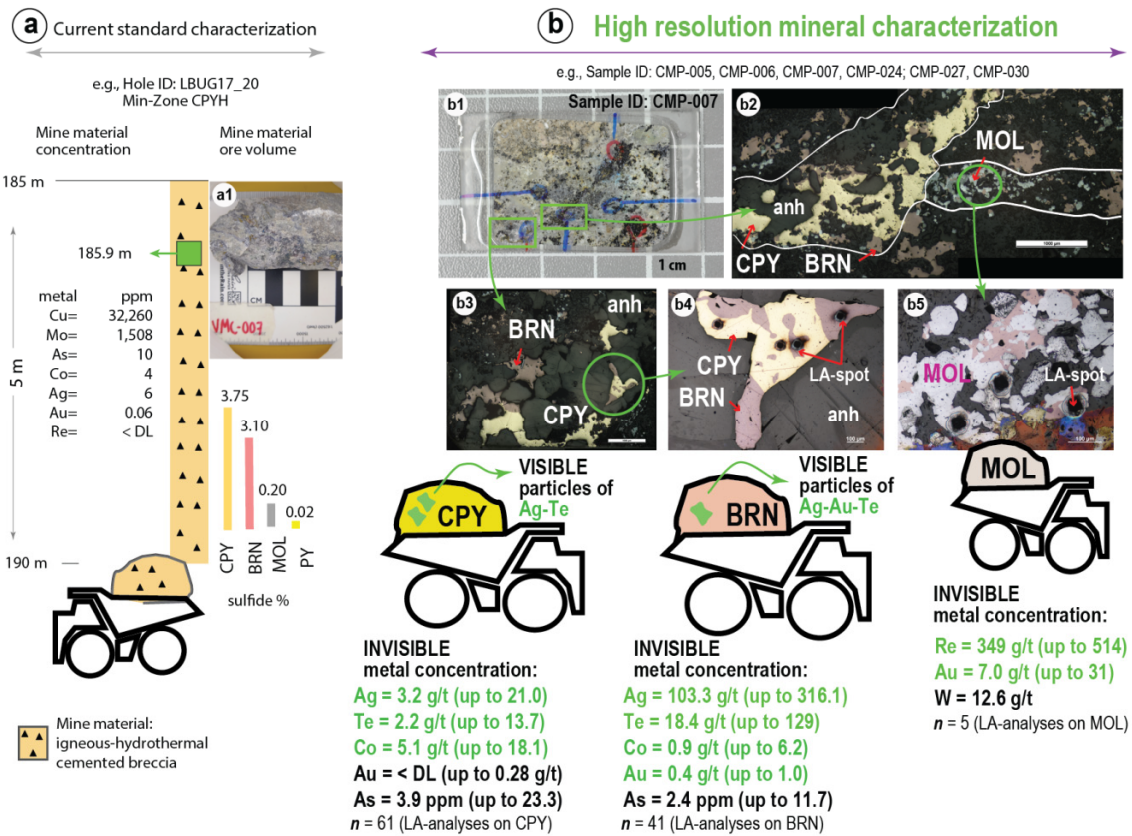


**Figure 5.** Schematic diagram illustrating: (a) current Cu-sulfide geochemical characterization, consisting of bulk geochemical analyses performed on 5 m-composite samples of mine material (on the right side a photograph is shown, a1). (b) The proposed high-resolution characterization for the GMU1, showing the mode of occurrence for each metal-bearing sulfide and the specific metal content, including the grade and mode of occurrence for metals.

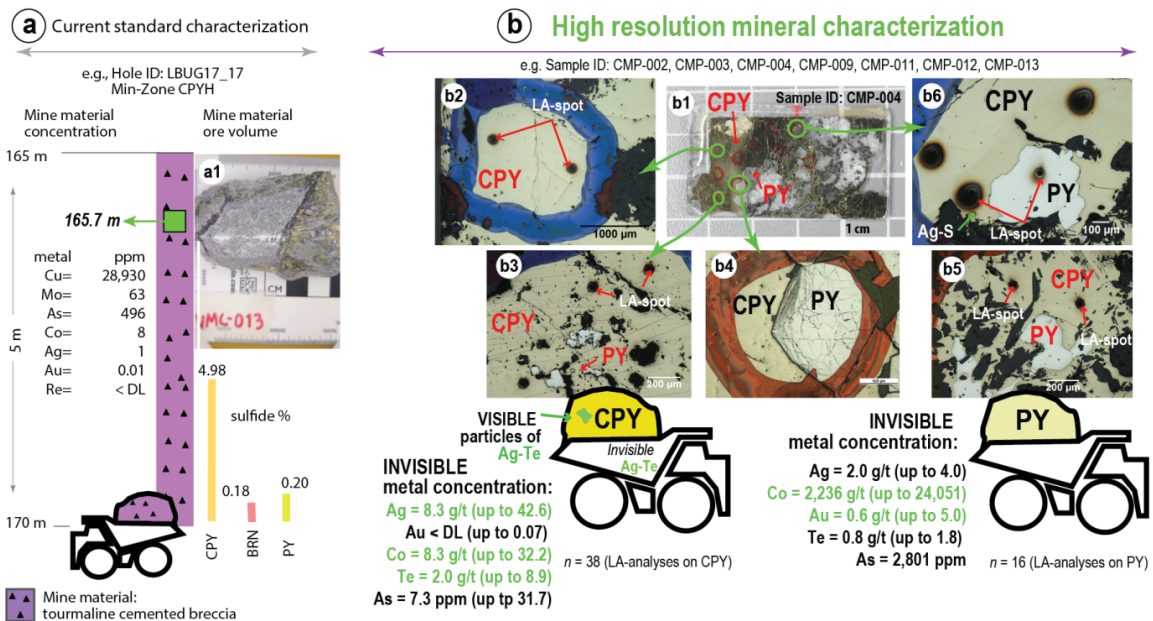


**Figure 6.** Schematic diagram illustrating: (a) the current Cu-sulfide ore characterization, which consist of bulk geochemical analyses performed on 5 m-composite samples of mine material (on the right side

photograph is shown, a1). (b) The proposed multi-metal high-resolution characterization for the GMU2, indicating the mode of occurrence for each metal-bearing sulfide and the specific metal content, including the grade and style of appearance of each metal.

From a standard standpoint, the GMU1 (Figure 5a) is characterized by a bulk trace-metal content of As = 10 ppm; Co = 4 ppm; Ag = 6 ppm; Au = 0.06 ppm; while Re and Te are present in concentrations below detection limits [39]. By implementing an advanced geochemical characterization (Table 1), the following strategic information can be obtained in our case study (Figure 5b): (1) bornite is the main host sulfide for trace Ag (up to 316 ppm) and Te (up to 129 ppm), and it also contains Au in concentrations of up to 1.0 ppm, results that are in agreement with the presence of micron-sized particles of Ag-Au-Te found as metallic inclusions. Bornite is almost depleted in Co and As trace elements, with concentrations of less than 6.2 ppm and 11.7 ppm, respectively; (2) chalcopyrite is enriched also with trace Ag (up to 21 ppm) and Te (up to 13.7 ppm); however, Au contents were below detection limits. In comparison with bornite, chalcopyrite is richer in trace Co (up to 18.1 ppm) and As (up to 23.3 ppm) concentrations; (3) molybdenite is a strategic host mineral for trace Au (up to 31 ppm), and also contains trace Re with an average grade of 349 ppm and ranging of up to 514 ppm. The aforementioned results represent significant metal content, which was not characterized by geochemical analysis performed on the bulk mine-material. Therefore, this metal content would not be considered in the standard ore processing design.

Standard geochemical characterization performed on the GMU2 samples (Figure 6a) shows that the bulk average for trace-elements concentrations of As = 496 ppm, Co = 8 ppm, Ag = 1 ppm; Au = 0.01 ppm and Re < DL [39]. The advanced geochemical characterization (Figure 6b; Table 2) shows that trace Co = 2236 ppm (up to 24,051 ppm), Au = 0.6 ppm (up to 5 ppm) and As = 2801 ppm (up to 6090 ppm) are preferentially contained in pyrite. In contrast, Ag is favorably concentrated in chalcopyrite (up to 42.6 ppm), being almost depleted in As = 7.3 ppm, Co = 8.3 ppm, and Au < DL, in comparison to pyrite. An important difference that arises from the advanced geochemical characterization is the mode of occurrence of As, which is not contained in chalcopyrite. However, bulk chemical results show As concentrations of around 500 ppm in the mine material, a metallic content that could erroneously penalize the Cu-grades of sulfide concentrates.

According to the standard characterization the GMU1 is richer in Ag concentration in relation to the GMU2 (GMU1 = 6 ppm Ag and GMU2 = 1 ppm Ag). However, the advanced geochemical characterization shows that chalcopyrite from GMU2 presents higher grade values for Ag (average of 8.3 ppm) in comparison with the chalcopyrite from GMU1 (average of 3.2 ppm). This silver behavior can be due to the absence of bornite in the GMU2, a mineral that preferentially concentrates Ag in its lattice [36]. Even if Ag (plus Au) is systematically dosed on prime minerals such as bornite and chalcopyrite, a remarkable data obtained from the advanced characterization is the mode of occurrence for these metals, i.e., Ag and Au, which are mainly found as Ag ( $\pm$ Au)-Te sulfosalts, instead of monometallic or electrum particles. This finding is fundamental to the development of metallurgical models.

#### 4.1. Metallurgical Processing and Opportunities for Precious and Critical Metal Supply

The results presented previously reveal that the geo-metallurgical units defined for copper extraction, e.g., GMU1 and GMU2 (Figures 5 and 6), also can contain critical and precious metals in trace but profitable concentrations. For instance, in our case study: (i) the GMU1 (Figure 5) is characterized by profitable trace Au and Re contents associated with molybdenite, and (ii) the GMU2 (Figure 6) contains trace Co and Au, with the profitable metal grades associated with pyrite. These trace metals could be recovered in the same copper processing workflow during sulfide flotation processes, by modification or inclusion of some additional unit operations. Our proposed improvements are addressed to sulfide flotation workflows because sulfide concentrates will become the main marketable product produce by the copper industry in Chile over the coming years, with an estimated increase of

47.8% by 2030 [40]. If profitable by-products are not recovered during flotation processes, they will be extracted later during electro-refining and electro-winning processes, or sent to tailings [10].

The common scenario for producing sulfide flotation concentrates is a processing plant consisting of crushing, grinding, bulk-sulfide flotation, and selective Cu-sulfide flotation. However, identification of critical and precious metals associated with a specific sulfide gives rise to opportunities to propose new processing plant workflows for recovering these trace metals, in addition to copper + molybdenum, as marketable products during the flotation processes. To develop the conceptual mass balance approach, the following assumptions are considered: (i) the elemental content of each metal is obtained from the bulk geochemical characterization performed on the head ore, i.e., the current standard characterization (e.g., Figures 5a and 6a). These values are represented in the flow of the ore fed into the crushing and grinding steps; (ii) the mass balance considers the association of each metal with its specific hosting mineral (e.g., Figures 5b and 6b); (iii) the mass balance incorporates the behavior of each metal-bearing mineral in the respective unit operation. Therefore, the result of each metal of interest will be determined by the behavior of its specific mineral association.

#### 4.1.1. Re and Au from Molybdenite

For the GMU1, the mass balance in a conventional processing plant (Figure 7) is designed to produce copper and molybdenum concentrates. In this case, a concentration factor of 10 is expected in the bulk flotation concentrate if an ideal separation between molybdenite and other sulfide minerals is reached [15].

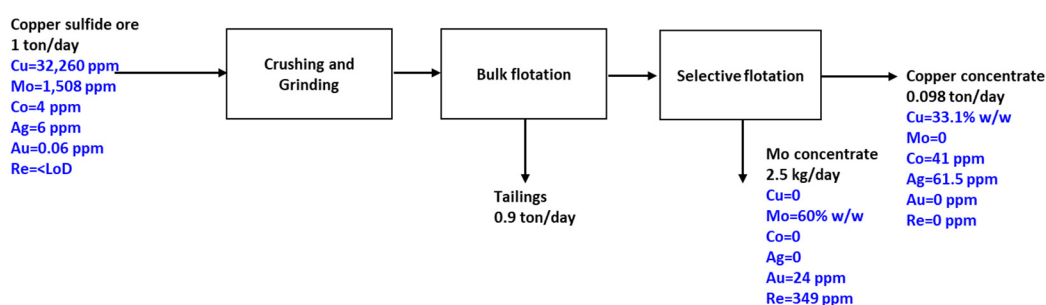


**Figure 7.** Schematic flow-sheet for a conventional plant design to treat porphyry ores, by processing mine material from the GMU1, to produce copper and molybdenum concentrates.

For molybdenite concentrates, only the molybdenum content is accounted for in the final price of this marketable product. To evaluate the feasibility of additional extraction of by-products, i.e., Re and Au, we present a process, typically used to recover Mo [15], and how it can be modified to also extract trace Re and particularly Au contents from molybdenite (Figure 8).

Roasting of molybdenite concentrate is implemented to obtain  $\text{MoO}_3$  in the calcine, while  $\text{Re}_2\text{O}_7$  is accumulated in the gas stream. The calcine, which also would contain gold, can be further treated with ammonia to dissolve the  $\text{MoO}_3$  and transform it in the ammonium molybdate. At this stage, it is essential to consider that ammonia can dissolve gold under oxidative conditions; therefore, a rigorous control of the dissolved oxygen must be performed [15]. In spite of this, operational temperatures of this  $\text{MoO}_3$  leaching (40–80 °C) are lower than those typically measured for ammonia leaching of gold (>80 °C) [41]. Therefore, this parameter can be operationally controlled. Finally, the leaching residue which contains gold can be treated in the proposed pathway by cyanidation and carbon adsorption to produce *dore metal* as a marketable product (Figure 8).

In the Re pathway, the ammonium molybdate solution can be crystallized to obtain ammonium dimolybdate, which is the final product typically generated from molybdenite concentrates (Figure 8). The gases containing rhenium ( $\text{Re}_2\text{O}_7$ ), which are generated during roasting, can be treated in a scrubbing gas system to obtain a solution of perrhenic acid ( $\text{HReO}_4$ ), which, in turn, are sent to an ionic exchange (IX) process to recover rhenium as ammonium perrhenate ( $\text{NH}_4\text{ReO}_4$ ). The elution

stage of the IX process is performed with ammonia, in which the generated solutions are crystallized to obtain the ammonium perrhenate (Figure 8), another marketable product, along with the *dore metal* produced from this proposed UGM. The processing option described in Figure 8 is not very different from that conventionally implemented by molybdenum refineries, in which rhenium and gold contents are frequently recovered from molybdenum concentrates.

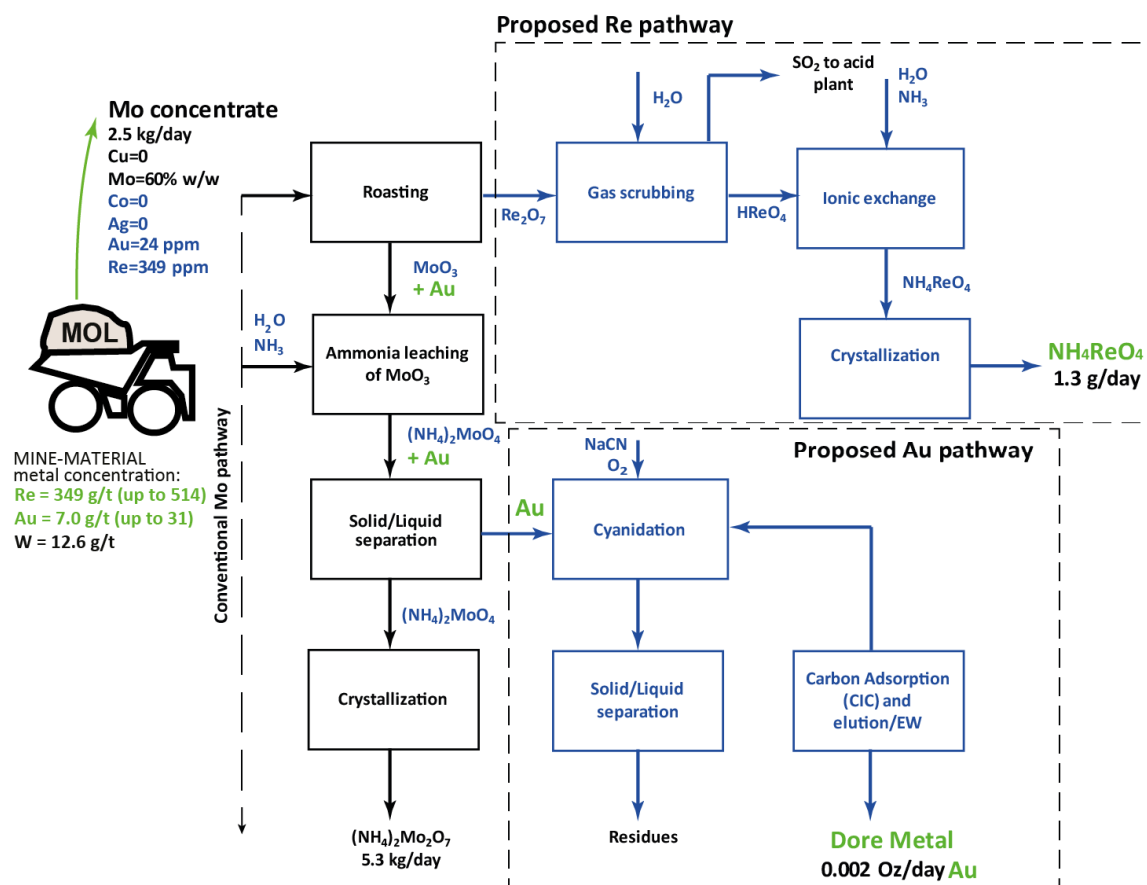


**Figure 8.** Schematic flow-sheet proposed to recover marketable critical and precious metals, such as Re and Au, in addition to Mo, from a molybdenite concentrate.

The presented mass balance (Figure 8) considers a unitary basis for the feed-ore, i.e., a unit estimation based on 1 ton of Cu-Mo sulfide ore processed per day, to easily scale-up to other treatment capacities. The scaling-up methodology can be expected as linear, assuming the recoveries are not affected. For instance, in a case of a plant design with a capacity setting at 140,000 t/day of head ore treatment (a typical capacity for the big mining), the gold, rhenium, and molybdenum production as by-products could reach up to 280 Oz/day (102,200 Oz/year), 122.8 kg/day (44,822 kg/year), and 211.1 ton/day (77,000 ton/year), respectively.

#### 4.1.2. Co and Au from Pyrite

The proposed UGM2 contains interesting grades of Co and Au, particularly concentrated in pyrite, a sulfide often not accounted for conventional process streams, which are designed to produce Cu and Mo-sulfide concentrates (Figure 9).

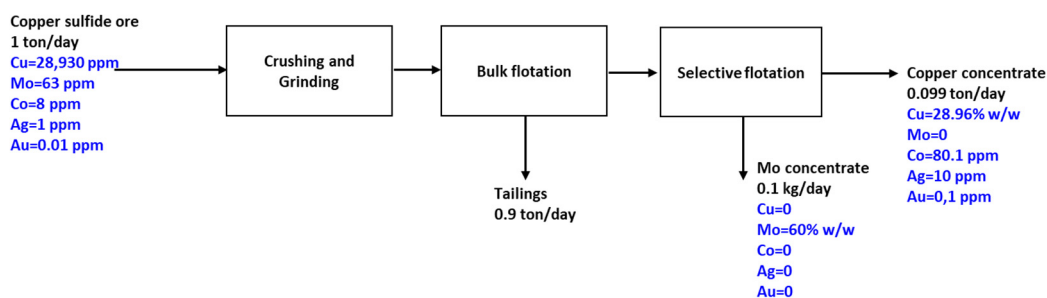


**Figure 9.** Schematic flow-sheet for a conventional plant design to treat porphyry ores, by processing mine material from the GMU2, to produce copper and molybdenum concentrates.

These concentrates are typically sold to a refinery furnace, which do not contain only Cu and Mo. Copper concentrates may include pyrite, which contains Co and Au (+Ag, ±Te), although generally only Au and Ag are valued in the concentrate selling price.

Considering that Co and Au trace concentrations are mainly contained in pyrite (Figure 6), there is an opportunity to modify the Cu processing design by the addition of a pyrite depression flotation stage (Figure 10). Thus, it is possible to separate pyrite from the other sulfides [42], which in our case study is chalcopyrite. Then, a pyrite concentrate can be generated and processed to recover Co and Au as marketable products (Figure 10), before sending pyrite to the tailings together with its metallic content [10]. In the proposed schematic flow-sheet (Figure 10), mass balance assumes ideal separation efficiency for each unit operation [15].

In the proposed pathway, pyrite concentrates can be treated in an oxidative environment to liberate Co and Au from the refractory sulfide matrix, considering that trace Co and Au are concentrated in nano-particles or in the mineral lattice. Here, an issue to be controlled is the percent of recoveries for Co and Au during the downstream stages. For that, it is best to incorporate an additional operational unit consisting of typical oxidative pretreatments [16], including roasting, bioleaching, pressure leaching, and oxidative acid leaching processes, which are systematically used to extract metallic Au from refractory minerals. In this way, it has recently been shown [43] that invisible Au in pyrite can be contained in an adsorbed state in the form of S-Au-S clusters, in contrast to the existing view that Au replaces Fe or S in the mineral lattice [44]. Thus, adsorbed Au is much less stable and, therefore, more easily recoverable by existing processes than the Au bound to the lattice [43]. In the case of roasting, an acid leaching of calcine must be included to dissolve the CoO formed during this process. Then, the pregnant leach solution (PLS), which will contain Co, Fe, and sulfuric acid, can be treated in a solid-liquid separation stage to remove the insoluble compounds from the PLS. Finally, insoluble compounds can be treated by cyanidation, a typical process to dissolve gold, and followed by a carbon adsorption process in pulp (CIP), including the correspondent elution and electro-winning (EW) stages [16]. Depending on the tonnage of mine material to be processed, it can also be recommended the use of an alternative carbon in column (CIC) after filtration.

In the other branch of the proposed flow-sheet, the PLS containing cobalt can be processed in a fractional stage to remove impurities, such as Fe, Cu, acid, and magnesium, and using specific pH conditions for each element [15,45,46]. Cobalt can be recovered as  $\text{Co}(\text{OH})_2$  after precipitation with MgO. Alternative processes for treating the PLS, such as solvent extraction, crystallization, or EW, can be evaluated to obtain different Co products, depending on the impurities contained and reagents price [45,46].

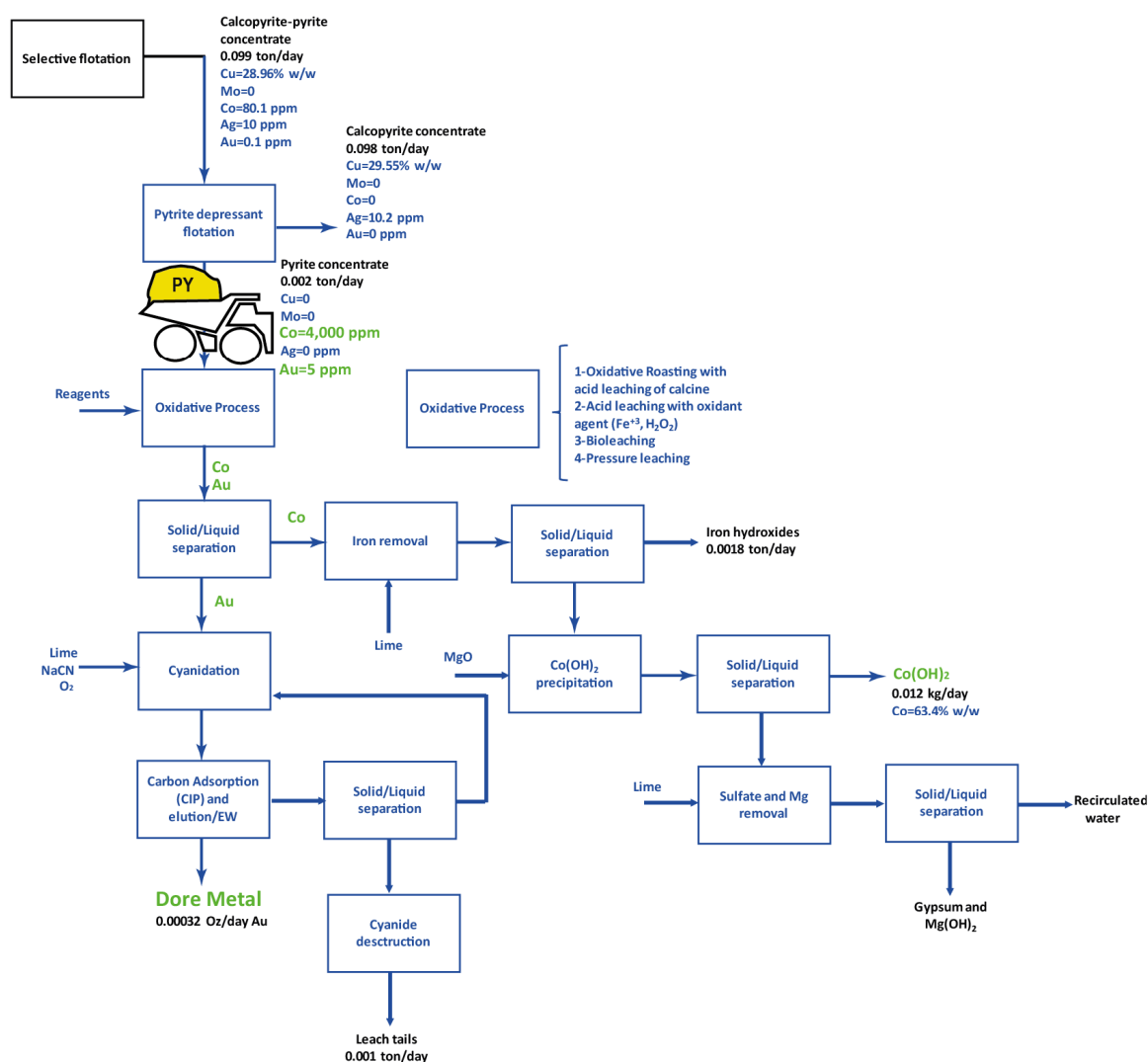


**Figure 10.** Schematic flow-sheet proposed to recover marketable critical metals, such as Co and Au from a pyrite concentrate, during sulfide concentrate production.

The process depicted in Figure 10 shows a significant reduction of the material volume to be treated from a pyrite concentrate (0.2% of the head ore), during the sulfide concentrate production. It has an additional positive effect, which is a remarkable increase of Co and Au grades up to 4000 and 5 g/t, respectively. Interestingly, the cost of mining, crushing, and grinding stages, developed on the bulk mine-material, are accounted into the copper production investments, which would imply that only the value for implementing additional operation units must be imputed to the by-products budget. Additionally, the reduction of the material to be processed can facilitate the installation of additional operation units in the same work areas previously designated to metallurgical plants. Considering a similar plant design with a head-ore treatment of 140,000 t/day, the by-products benefit could reach up to 44.8 Oz/day for Au (16,352 Oz/year), and 1065 kg/day for Co (389 t/year), which is a metal content not considered in the current mining plan. Therefore, future work must be focused on demonstrating, at a laboratory scale, the metal recoveries determined from a conceptual approach.

## 5. Concluding Remarks

In this study, we have shown that the metallic potential that could be assessed from a porphyry-type mining operation and how a high-resolution geochemical characterization of sulfides can be used to determine the concentration of trace metals as by-products. Critical and precious metals, such as Co,

Au, Re, Ag, and Te contained in ore sulfides, which are necessary for the development of society in the coming decades, are often not considered in mining planning and would be lost to tailings [10] or in the refineries wastes.

Even if the multi-metallic enrichment in porphyry-type deposits is well-known [10,12–14], very little work has been published on the metallurgical processing of these trace metals during the production of Cu- and Mo-concentrates. To our knowledge, a significant constraint to evaluate such possibility is the geochemical information obtained in operational chemical analyses, which is focused on copper contents [10]. Thus, recently, economic geologists are turning their interest in the detection of trace element concentrations directly in Cu-ore samples [47], and in evaluating possibilities to extract trace metals as by-products during Cu-sulfide processing [48] associated with sulfide concentrates production.

Here, we propose work-sheets to evaluate critical and precious metals processing during the production of sulfide concentrates, by the addition of some specific unit operations to conventional metallurgical concentrator plant designs. The advantages to be considered are as follows:

1. Millions of tons of mining material are processed each year by the porphyry mining industry, generating the possibility of beneficiation of by-product content, even if some metals are found in very low concentrations such as parts per million;
2. Investments for the extraction and processing of the mined material are reflected in the price of copper, and therefore only the additional unit operations could be taken into account in the economic assessment of the feasibility processing the by-products;
3. The identification of the specific mineral hosting each metal in trace amounts makes it possible to design a metallurgical treatment with quantities of material several times smaller than those represented by the treatment of Cu and Mo. For example, molybdenite and pyrite represent only 0.2% of the bulk material of GMU1 and GMU2, respectively. This idea implies that additional operational units can be installed in situ in the mining operations, avoiding the carrying of mined material;
4. The pyrite depression process, proposed to obtain a pyrite concentrate, can be applied both to extract the Co and Au contents of the pyrite and to reduce the amount of pyrite sent to the tailings. The latter is important from an environmental perspective because pyrite being a reactive mineral, its exposure to oxygen and water can facilitate the oxidative dissolution of the sulfide structure, resulting in acid mine drainage (AMD) [49]. The proposed workflows take into account the metallurgical processing of a recognized metal-bearing mineral, such as the processing of pyrite to obtain Co and Au, in conjunction with concentrate production. The latter idea can help reduce the amount of material to be processed, compared with a subsequent recovery of metals, such as Co, from mine tailings [49,50].

Thus, an economic evaluation can be made by considering the cost of setting up a plant similar to what we are proposing and comparing it with to the selling price of Cu and Mo concentrates, in which the trace metals contained would be valued in the final prices, i.e., Co and Au for Cu concentrates, and Re and Au for Mo concentrates.

**Author Contributions:** Conceptualization, G.V.; methodology, G.V. and S.S.; validation, I.V., S.S. and M.P.; formal analysis, G.V.; investigation, G.V. and H.E.; resources, G.V., I.V. and M.P.; writing-original draft preparation, G.V. and H.E.; writing-review and editing, S.S., I.V. and M.P.; visualization, G.V.; supervision, I.V.; project administration, G.V., M.P., and S.S.; funding acquisition, G.V. All authors have read and agree to the published version of the manuscript.

**Funding:** This research was partially funded by the National Commission for Scientific and Technological Research (CONICYT Chile) through CONICYT-PIA Project AFB180004.

**Acknowledgments:** We are grateful to S. Gouy and Ph. de Parseval for their help during SEM and EMP analyses at the Centre de Micro-Characterisation Raimond Castaing (UMS 3623) in Toulouse, France, and T. Aigouy for their help during the SEM analyses at the GET Laboratory in Toulouse, France. We would also like to thank J. Chmeleff and C. Duquenoey for their technical assistance on the LA-ICP-MS analyses at the GET Laboratory. G. Velásquez

and H. Estay acknowledge the National Commission for Scientific and Technological Research (CONICYT Chile), through CONICYT-PIA Project AFB180004 they were benefited to conduct part of this research. Constructive comments by two anonymous reviewers substantially improved the quality of this manuscript.

**Conflicts of Interest:** The authors declare no conflict of interest.

## References

1. Mudd, G.M.; Weng, Z.; Jowitt, S.M. A detailed assessment of global Cu resource trends and endowments. *Econ. Geol.* **2013**, *108*, 1163–1183. [[CrossRef](#)]
2. Calvo, G.; Mudd, G.; Valero, A.; Valero, A. Decreasing ore grades in global metallic mining: A theoretical issue or a global reality? *Resources* **2016**, *5*, 36. [[CrossRef](#)]
3. Meinert, L.; Robinson, G.; Nassar, N. Mineral resources: Reserves, peak production and the future. *Resources* **2016**, *5*, 14. [[CrossRef](#)]
4. Moreau, V.; Dos Reis, P.C.; Vuille, F. Enough metals? Resource constraints to supply a fully renewable energy system. *Resources* **2019**, *8*, 29. [[CrossRef](#)]
5. Grandell, L.; Lehtilä, A.; Kivinen, M.; Koljonen, T.; Kihlman, S.; Lauri, L.S. Role of critical metals in the future markets of clean energy technologies. *Renew. Energy* **2016**, *95*, 53–62. [[CrossRef](#)]
6. Watari, T.; McLellan, B.C.; Giurco, D.; Dominish, E.; Yamasue, E.; Nansai, K. Total material requirement for the global energy transition to 2050: A focus on transport and electricity. *Resour. Conserv. Recycl.* **2019**, *148*, 91–103. [[CrossRef](#)]
7. Schipper, B.W.; Lin, H.-C.; Meloni, M.A.; Wansleebend, K.; Heijungs, R.; van der Voet, E. Estimating global copper demand until 2100 with regression and stock dynamics. *Resour. Conserv. Recycl.* **2018**, *132*, 28–36. [[CrossRef](#)]
8. McFall, K.; Roberts, S.; McDonald, I.; Boyce, A.J.; Naden, J.; Teagle, D. Rhenium enrichment in the Muratdere Cu-Mo (Au-Re) porphyry deposit, Turkey: Evidence from stable isotope analyses ( $\delta^{34}\text{S}$ ,  $\delta^{18}\text{O}$ ,  $\delta\text{D}$ ) and laser ablation-inductively coupled plasma-mass spectrometry analysis of sulfides. *Econ. Geol.* **2019**, *114*, 1443–1466. [[CrossRef](#)]
9. Northey, S.; Mohr, S.; Mudd, G.M.; Weng, Z.; Giurco, D. Modelling future copper ore grade decline based on a detailed assessment of copper resources and mining. *Resour. Conserv. Recycl.* **2014**, *83*, 190–201. [[CrossRef](#)]
10. Velásquez, G.; Carrizo, D.; Salvi, S.; Vela, I.; Pablo, M.; Pérez, A. Tracking cobalt, REE and gold from porphyry copper deposits by LA-ICP-MS: A geological approach towards metal-selective mining in tailings. *Minerals* **2020**, *10*, 109. [[CrossRef](#)]
11. Nurmi, P.A. Green mining—A holistic concept for sustainable and acceptable mineral production. *Ann. Geophys.* **2017**, *60*. [[CrossRef](#)]
12. Kesler, S.E.; Chryssoulis, S.L.; Simon, G. Gold in porphyry copper deposits: Its abundance and fate. *Ore Geol. Rev.* **2002**, *21*, 103–124. [[CrossRef](#)]
13. Voudouris, P.; Melfos, V.; Spry, P.G.; Bindi, L.; Moritz, R.; Ortelli, M.; Kartal, T. Extremely Re-rich molybdenite from porphyry Cu-Mo-Au prospects in northeastern Greece: Mode of occurrence, causes of enrichment, and implications for gold exploration. *Minerals* **2013**, *3*, 165–191. [[CrossRef](#)]
14. Crespo, J.; Reich, M.; Barra, F.; Verdugo, J.J.; Martínez, C. Critical metal particles in copper sulfides from the supergiant Río Blanco porphyry Cu-Mo deposit, Chile. *Minerals* **2018**, *8*, 519. [[CrossRef](#)]
15. Habashi, F. *Handbook of Extractive Metallurgy*; Wiley-VCH: Weinheim, Germany, 1997.
16. Marsden, J.O.; House, C.I. *The Chemistry of Gold Extraction*, 2nd ed.; The Society of Mining, Metallurgy, and Exploration Inc. (SME): Colorado, CO, USA, 2006.
17. Escolme, A.; Berry, R.F.; Hunt, J.; Halley, S.; Potma, W. Predictive models of mineralogy from whole-rock assay data: Case study from the Productora Cu-Au-Mo deposit, Chile. *Econ. Geol.* **2019**, *114*, 1513–1542. [[CrossRef](#)]
18. Irarrazaval, V.; Sillitoe, R.H.; Wilson, A.J.; Toro, J.C.; Robles, W.; Lyall, G. Discovery history of a giant, high-grade, hypogene porphyry copper-molybdenum deposit at Los Sulfatos, Los Bronces-Río Blanco District, Central Chile. In *The Challenge of Finding New Mineral Resources: Global Metallogeny, Innovative Exploration, and New Discoveries*; Goldfarb, R.J., Marsh, E.E., Monecke, T., Eds.; Special Publications of the Society of Economic Geologists: Littleton, CO, USA, 2010; Volume 15, pp. 253–269.



19. Toro, J.C.; Ortúzar, J.; Zamorano, J.; Cuadra, P.; Hermosilla, J.; Spröhnle, C. Protracted magmatic-hydrothermal history of the Río Blanco-Los Bronces district, Central Chile: Development of world's greatest known concentration of copper. In *Geology and Genesis of Major Copper Deposits and Districts of the World: A Tribute to Richard H. Sillitoe*; Hedenquist, J.W., Harris, M., Camus, F., Eds.; Special Publications of the Society of Economic Geologists: Littleton, CO, USA, 2012; Volume 16, pp. 105–126.
20. Deckart, K.; Silva, W.; Spröhnle, C.; Vela, I. Timing and duration of hydrothermal activity at the Los Bronces porphyry cluster: An update. *Miner. Depos.* **2014**, *49*, 535–546. [[CrossRef](#)]
21. Bensalah, N.; Dawood, H. Review on synthesis, characterizations, and electrochemical properties of cathode materials for lithium ion batteries. *J. Mater. Sci. Eng.* **2016**, *5*, 4. [[CrossRef](#)]
22. Ghatak, K.; Basu, S.; Das, T.; Kumar, H.; Datta, D. Effect of cobalt content on the electrochemical properties and structural stability of NCA type cathode materials. *Phys. Chem. Chem. Phys.* **2018**, *20*, 22805–22817. [[CrossRef](#)]
23. Kesler, S.E.; Gruber, P.W.; Medina, P.A.; Keoleian, G.A.; Everson, M.P.; Wallington, T.J. Global lithium resources: Relative importance of pegmatites, brine and other deposits. *Ore Geol. Rev.* **2012**, *48*, 55–69. [[CrossRef](#)]
24. Munk, L.A.; Hynek, S.A.; Bradley, D.; Boutt, D.; Labay, K.; Jochens, H. Lithium brines: A global perspective. *Rev. Econ. Geol.* **2016**, *18*, 339–365.
25. Berzina, A.N.; Sotnikov, V.I.; Economou-Eliopoulos, M.; Eliopoulos, D.G. Distribution of rhenium in molybdenite from porphyry Cu-Mo and Mo-Cu deposits of Russia (Siberia) and Mongolia. *Ore Geol. Rev.* **2005**, *26*, 91–113. [[CrossRef](#)]
26. Cabri, L.J.; Chryssoulis, S.L.; de Villiers, J.P.R.; Laflamme, J.H.G.; Buseck, P.R. The nature of “invisible” gold in arsenopyrite. *Can. Mineral.* **1989**, *27*, 353–362.
27. Riesner, M.; Simoes, M.; Carrizo, D.; Lacassin, R. Early exhumation of the Frontal Cordillera (Southern Central Andes) and implications for Andean mountain-building at ~33.5° S. *Sci. Rep.* **2019**, *9*, 7972. [[CrossRef](#)] [[PubMed](#)]
28. Cook, N.; Ciobanu, C.L.; George, L.; Zhu, Z.-Y.; Wade, B.; Ehrig, K. Trace element analysis of minerals in magmatic-hydrothermal ores by laser ablation inductively-coupled plasma mass spectrometry: Approaches and opportunities. *Minerals* **2016**, *6*, 111. [[CrossRef](#)]
29. Velásquez, G.; Béziat, D.; Salvi, S.; Siebenaller, L.; Borisova, A.Y.; Pokrovski, G.S.; De Parseval, P. Formation and deformation of pyrite and implications for gold mineralization in the El Callao District, Venezuela. *Econ. Geol.* **2014**, *109*, 457–486. [[CrossRef](#)]
30. Velásquez, G.; Borisova, A.Y.; Salvi, S.; Béziat, D. In situ determination of Au and Cu in natural pyrite by near-infrared femtosecond laser ablation-inductively coupled plasma-quadrupole mass spectrometry: No Evidence for matrix effects. *Geostand. Geoanal. Res.* **2012**, *36*, 315–324. [[CrossRef](#)]
31. Borisova, A.; Thomas, R.; Salvi, S.; Candaudap, F.; Lanzanova, A.; Chmeleff, J. Tin and associated metal and metalloid geochemistry by femtosecond LA-ICP-QMS microanalysis of pegmatite-leucogranite melt and fluid inclusions: New evidence for melt-melt-fluid immiscibility. *Mineral. Mag.* **2012**, *76*, 91–113. [[CrossRef](#)]
32. Van Achterbergh, E.; Ryan, C.G.; Griffin, W.L. *Data Reduction Software for LA-ICP-MS*; Mineralogical Association of Canada Short Course Notes: Calgary, AB, Canada, 2001; Volume 29, pp. 239–243.
33. Sylvester, P.J.; Cabri, L.J.; Tubrett, M.N.; McMahon, G.; Laflamme, J.H.G.; Peregoedova, A. Synthesis and evaluation of a fused pyrrhotite standard reference material for platinum group element and gold analysis by laser ablation-ICP-MS. In Proceedings of the 10th International Platinum Symposium, Oulu, Finland, 8–11 August 2005; pp. 16–20.
34. Pearce, N.J.; Perkins, W.T.; Westgate, J.A.; Gorton, M.P.; Jackson, S.E.; Neal, C.R.; Chenery, S.P. A compilation of new and published major and trace element data for NIST SRM 610 and NIST SRM 612 glass reference materials. *Geostand. Geoanal. Res.* **1997**, *21*, 115–144. [[CrossRef](#)]
35. Long, G.; Peng, Y.; Bradshaw, D. A review of copper–arsenic mineral removal from copper concentrates. *Min. Eng.* **2012**, *36–38*, 179–186. [[CrossRef](#)]
36. Ciobanu, C.L.; Cook, N.J.; Kelson, C.R.; Guerin, R.; Kalleske, N.; Danyushevsky, L. Trace element heterogeneity in molybdenite fingerprints stages of mineralization. *Chem. Geol.* **2013**, *347*, 175–189. [[CrossRef](#)]
37. Deditius, A.P.; Utsunomiya, S.; Reich, M.; Kesler, S.E.; Ewing, R.C.; Hough, R.; Walshe, J. Trace metal nanoparticles in pyrite. *Ore Geol. Rev.* **2011**, *42*, 32–46. [[CrossRef](#)]

38. Sykora, S.; Cooke, D.R.; Meffre, S.; Stephanov, A.S.; Gardner, K.; Scott, R.; Selley, D.; Harris, A.C. Evolution of pyrite trace element compositions from porphyry-style and epithermal conditions at the Lihir gold deposit: Implications for ore genesis and mineral processing. *Econ. Geol.* **2018**, *113*, 193–208. [[CrossRef](#)]
39. Anglo American Sur, S.A. Bulk chemical assays database, until 2019. Los Sulfatos Mine-Material. The Los Bronces Underground Project. Internal Report.
40. COCHILCO-Comision Chilena del Cobre. Proyección de la Producción de Cobre en Chile 2019–2030. DEPP 15/2019. Registro Propiedad Intelectual N° 310805: Santiago, Chile, 2019; p. 43. Available online: <https://www.cochilco.cl/Listado%20Temtico/Proyecci%C3%B3n%20de%20la%20producci%C3%B3n%20esperada%20de%20cobre%202019%20-%202030%20Vfinal.pdf> (accessed on 20 March 2020).
41. Aylmore, M.G. Alternative Lixivants to Cyanide for Leaching Gold Ores. Chapter 27. In *Gold Ore Processing: Project Developments and Operations*, 2nd ed.; Adams, M.D., Ed.; Elsevier: Amsterdam, The Netherlands, 2016.
42. Mu, Y.; Peng, Y.; Lauten, R.A. The depression of pyrite in selective flotation by different reagent systems—A Literature review. *Miner. Eng.* **2016**, *96–97*, 143–156. [[CrossRef](#)]
43. Pokrovski, G.S.; Kokh, M.A.; Proux, O.; Hazemann, J.-L.; Bazarkina, E.F.; Testemale, D.; Escoda, C.; Boiron, M.-C.; Blanchard, M.; Aigou, T.; et al. The nature and partitioning of invisible gold in the pyrite-fluid system. *Ore Geol. Rev.* **2019**, *109*, 545–563. [[CrossRef](#)]
44. Simon, G.; Huang, H.; Penner-Hahn, J.E.; Kesler, S.E.; Kao, L. Oxidation state of gold and arsenic in gold-bearing arsenian pyrite. *Am. Mineral.* **1999**, *84*, 1071–1079. [[CrossRef](#)]
45. Sole, K.C.; Parker, J.; Cole, P.M.; Mooiman, M.B. Flowsheet options for cobalt recovery in African copper-cobalt hydrometallurgy circuits. *Min. Proc. Extr. Metall. Rev.* **2019**, *40*, 194–206. [[CrossRef](#)]
46. Shengo, M.L.; Kime, M.-B.; Mambwe, M.P.; Nyembo, T.K. A review of the beneficiation of copper-cobalt-bearing minerals in the Democratic Republic of Congo. *J. Sustain. Min.* **2019**, *18*, 226–246. [[CrossRef](#)]
47. Rollog, M.; Cook, N.J.; Guagliardo, P.; Ehrig, K.; Ciobanu, C.L.; Kilburn, M. Detection of Trace Elements/Isotopes in Olympic Dam Copper Concentrates by nanoSIMS. *Minerals* **2019**, *9*, 336. [[CrossRef](#)]
48. Schmandt, D.S.; Cook, N.J.; Ehrig, K.; Gilbert, S.; Wade, B.P.; Rollog, M.; Ciobanu, C.L.; Kamenetsky, V.S. Uptake of trace elements by baryte during copper ore processing: A case study from Olympic Dam, South Australia. *Miner. Eng.* **2019**, *135*, 83–94. [[CrossRef](#)]
49. Falagán, C.; Grail, B.M.; Barrie-Johnson, D. New approaches for extracting and recovering metals from mine tailings. *Miner. Eng.* **2017**, *106*, 71–78. [[CrossRef](#)]
50. Ahmadi, A.; Khezri, M.; Akbar-Abdollahzadeh, A.; Askari, M. Bioleaching of copper, nickel and cobalt from the low grade sulfidic tailing of Golgohar Iron Mine, Iran. *Hydrometallurgy* **2015**, *154*, 1–8. [[CrossRef](#)]



© 2020 by the authors. Licensee MDPI, Basel, Switzerland. This article is an open access article distributed under the terms and conditions of the Creative Commons Attribution (CC BY) license (<http://creativecommons.org/licenses/by/4.0/>).